DOI: 10.1002/cmdc.200500059

Structural Basis for the Exceptional in vivo Efficacy of Bisphosphonate Drugs

Jean-Michel Rondeau,*[a] Francis Bitsch,[a] Emmanuelle Bourgier,[a] Martin Geiser,[a] Rene Hemmig,[a] Markus Kroemer,[a] Sylvie Lehmann,[a] Paul Ramage,[a] Sebastien Rieffel,[a] André Strauss,[a] Jonathan R. Green,[b] and Wolfgang Jahnke*[a]

To understand the structural basis for bisphosphonate therapy of bone diseases, we solved the crystal structures of human farnesyl pyrophosphate synthase (FPPS) in its unliganded state, in complex with the nitrogen-containing bisphosphonate (N-BP) drugs zoledronate, pamidronate, alendronate, and ibandronate, and in the ternary complex with zoledronate and the substrate isopentenyl pyrophosphate (IPP). By revealing three structural snapshots of the enzyme catalytic cycle, each associated with a distinct conformational state, and details about the interactions with N-BPs, these structures provide a novel understanding of the mechanism of FPPS catalysis and inhibition. In particular, the accumulating substrate, IPP, was found to bind to and stabilize the FPPS–N-BP complexes rather than to compete with and displace the N-BP inhibitor. Stabilization of the FPPS–N-BP complex through IPP binding is supported by differential scanning calorimetry analyses of a set of representative N-BPs. Among other factors such as high binding affinity for bone mineral, this particular mode of FPPS inhibition contributes to the exceptional in vivo efficacy of N-BP drugs. Moreover, our data form the basis for structure-guided design of optimized N-BPs with improved pharmacological properties.

Introduction

Bisphosphonates are potent inhibitors of osteoclastic activity that are now widely used for preventing the bone loss associated with osteoporosis,[1] Paget's disease,[2] hypercalcemia[3] and metastatic bone disease.[4] At the biochemical level, there is now convincing evidence that the nitrogen-containing bisphosphonates (N-BPs, Figure 1a) inhibit the mevalonate pathway in osteoclasts and macrophages.[5,6] A key enzyme in the mevalonate pathway, farnesyl pyrophosphate synthase (FPPS), is thought to be the main molecular target of N-BPs,[7–9] but the precise interaction between N-BPs and the human enzyme has remained elusive.

Human FPPS, a homodimeric enzyme of 41-kDa subunits, catalyzes the two-step synthesis of the C_{15} metabolite farnesyl pyrophosphate (FPP) from the C_5 isoprenoids dimethylallyl pyrophosphate (DMAPP) and isopentenyl pyrophosphate (IPP, Figure 1b). FPP is required for the posttranslational prenylation of essential GTPase signalling proteins such as Ras and Rho[10] and is also a precursor for the synthesis of cholesterol, dolichol, and ubiquinone. Early biochemical studies have indicated that the FPPS reaction is Mg^{2+}- or Mn^{2+}-dependent and follows an ordered ternary-complex mechanism in which the allylic substrate binds first to the enzyme, then proceeds through the formation of an allylic carbocation, leading to the formation of the next higher homologue of the allylic substrate with concomitant release of pyrophosphate (PP_i).[11] Crystal structures of apo- and substrate-bound avian FPPS (42 kDa, 69% sequence identity to the human enzyme) have long served as a basis for the understanding of FPPS structure and mechanism.[12,13] However, recent X-ray analyses of *E. coli* FPPS (32 kDa, 25% sequence identity) and *S. aureus* FPPS (32 kDa, 27% sequence identity) showed marked differences in enzyme conformation, the number of metal sites, the binding mode of the allylic substrate, and the role of the conserved DDXXD motifs.[14] The extent to which conclusions from the avian or *E. coli* FPPS structures can be transferred to human FPPS remains unclear.[15] Herein, we provide the first experimental structures of human FPPS and present a differential scanning calorimetry (DSC) analysis of the binding of a set of representative N-BPs. Our data unveil three distinct conformational states of human FPPS and reveal that the exceptional efficacy of N-BP drugs stems, at least in part, from the stabilization of the inhibited complex by the accumulating homoallylic substrate.

[a] *Dr. J.-M. Rondeau, Dr. F. Bitsch, E. Bourgier, Dr. M. Geiser, R. Hemmig, Dr. M. Kroemer, S. Lehmann, Dr. P. Ramage, S. Rieffel, Dr. A. Strauss, Dr. W. Jahnke*
Novartis Institutes for BioMedical Research
Discovery Technologies
4002 Basel (Switzerland)
Fax: (+41) 61-324-2686
E-mail: jeanmichel.rondeau@novartis.com
wolfgang.jahnke@novartis.com

[b] *Dr. J. R. Green*
Novartis Institutes for BioMedical Research
Musculoskeletal Diseases
4002 Basel (Switzerland)

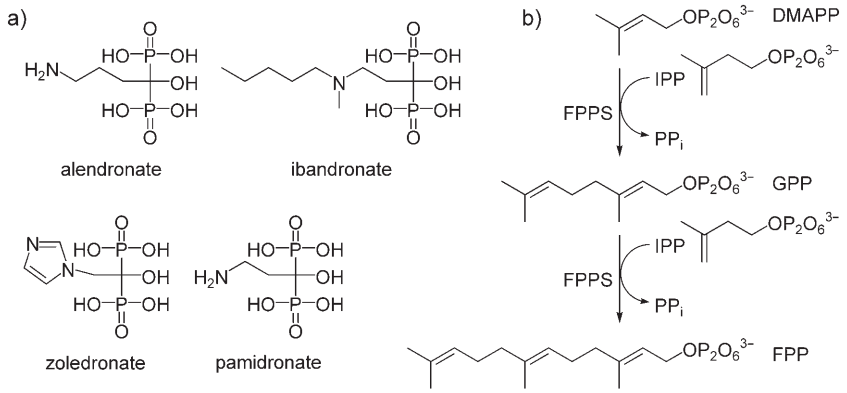

Figure 1. a) N-BP structures, all shown as the free acids; b) the mevalonate pathway: farnesyl pyrophosphate synthase (FPPS) catalyzes the two-step synthesis of farnesyl pyrophosphate (FPP) from isopentenyl pyrophosphate (IPP) and dimethylallyl pyrophosphate (DMAPP). GPP = geranyl pyrophosphate.

Results and Discussion

Overall structure: open, partially closed, and fully closed conformations

In comparison with the smaller microbial enzymes, avian and human FPPS possess three short helices (α-1, α-2 and α-3) inserted between helices H and I. Unliganded human FPPS adopts an open conformation very similar to that originally observed with the avian enzyme. In marked contrast, the complexes with the N-BP inhibitors and the ternary complex with zoledronate and IPP display closed conformations, which resemble that observed with the *E. coli* FPPS complexes, although substantial differences in the orientation of the I and J helices are apparent. This conformational switch in the human enzyme can be approximated by a rigid body motion of the last 130 C-terminal residues (Figure 2a) and involves a two-step mechanism. First, upon occupation of the allylic binding site, the two DDXXD motifs come closer together, and two loops (H–I and D–E) that line the substrate binding site form a "gate", which closes the entrance to the allylic binding site ("partially closed" conformation). This structural transition also requires a dramatic change in the orientation of the Tyr 349 side chain (Figure 2b). Second, upon IPP binding, the highly basic C-terminal tail of the enzyme (Lys 350, Arg 351, Arg 352, Lys 353), known to play a role in IPP binding and catalysis,[16] becomes ordered and clamps down to close the IPP binding site ("fully closed" conformation, Figure 2b). The open conformation facilitates product release and supports chain elongation by allowing translocation of geranyl pyrophosphate (GPP) to the allylic site and binding of a new IPP molecule for FPP synthesis in a processive mechanism. The partially closed conformation, triggered by occupation of the allylic binding site, fully forms the IPP binding site and thereby controls the order of DMAPP and IPP binding. It is mainly stabilized by electrostatic interactions between Lys 266 and Asp 107/Asp 174, and between the two DDXXD motifs, the three metal ions, and the pyrophosphate unit of the allylic substrate. The fully closed conformation, triggered by occupation of the IPP binding site and stabilized by electrostatic interactions between Lys 57 N^{ζ} and the C-terminal carboxylate group (Figure 2b), is catalytically active by orienting IPP and DMAPP correctly for reaction and by shielding from water the reactive carbocation intermediate formed during catalysis. The dimer interface is not affected by the conformational switch and constitutes a rigid core. Upon catalysis, release of pyrophosphate from the allylic substrate loosens the interactions with the DDXXD motifs, leading to destabilization of the closed conformation, transition to the open conformation, and resumption of the catalytic cycle.

Binary complexes with bisphosphonates

Alendronate, ibandronate, pamidronate, and zoledronate bind to the allylic substrate site and interact with both DDXXD motifs through a trinuclear metal centre (Figure 3). The binding of the bisphosphonate moiety is the same for all inhibitors. Three different divalent cations—Mg^{2+}, Mn^{2+}, and Zn^{2+}—were investigated in the work reported herein. With all three cations, the geometry and coordination of the metal cluster is conserved and is reminiscent of the trinuclear co-catalytic centres observed in some phosphatases,[17] nucleases,[18,19] and phospholipases.[20] Each metal site shows octahedral coordination involving the bisphosphonate oxygen atoms, the side-chain carboxylate groups of Asp 103, Asp 107 (first DDXXD motif) and Asp 243 (second DDXXD motif), and water molecules. The conserved residues Lys 200, Arg 112, and Lys 257 make direct salt-bridge interactions with the bisphosphonate moiety. Significantly, Lys 257 is part of the mobile H–I loop. Bisphosphonate binding therefore stabilizes the closed conformation of FPPS by interacting with both DDXXD motifs and Lys 257 of the H–I loop. The aliphatic amino group of pamidronate did not exhibit a well-defined electron density, suggesting that it does not make strong interactions with the enzyme active site, or adopts more than one orientation in the complex. In contrast, the imidazole substituent of zoledronate is well-ordered and makes strong interactions with FPPS: the protonated heterocyclic nitrogen atom makes a bifurcated H-bond interaction with Lys 200 (O) and Thr 201 ($O^{\gamma}1$), two conserved residues located at the kink of helix G which line the carbocation binding pocket (Figure 3). These interactions most likely contribute to the well-known preference for a nitrogen atom at the fourth position from the geminal carbon atom of the bisphosphonate moiety. The H-bonding interaction with $O^{\gamma}1$ of Thr 201 is also observed in the alendronate complex, but not with Lys 200 O. Pamidronate has its amino nitrogen atom in position 3 and hence cannot make any of these hydrogen bonds. Ibandronate also has its tertiary amino group in position 3 and does not form these hydrogen bonds; its methyl substituent makes van der Waals contacts with Thr 201 $O^{\gamma}1$ and Lys 200 O, where-

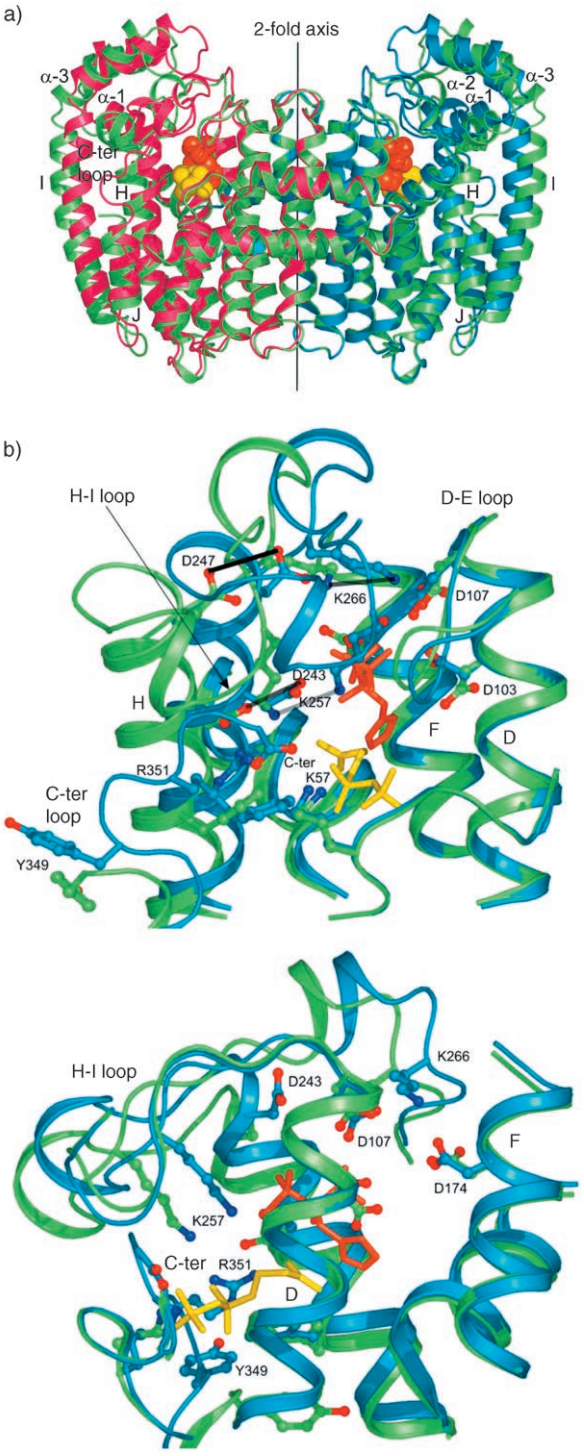

Figure 2. Conformational states of human FPPS. a) Overall view of the FPPS dimer in the fully closed conformation (IPP/zoledronate ternary complex, magenta/blue ribbon) and in the open conformation (unliganded, green ribbon). IPP (yellow) and zoledronate (orange) are shown in space-filling representation. b) Orthogonal views of the active site, showing the structural rearrangements between the open (green) and fully closed (blue) conformations with key residues highlighted. The positions of zoledronate and IPP in the fully closed conformation are shown in orange and yellow, respectively.

as its *n*-pentyl group is directed toward the FPPS dimer interface, filling a binding site thought to be normally occupied by the growing isoprenoid chain. The binding of the long ibandronate side chain is accompanied by conformational changes in the side chains of Phe 99, Thr 167, and Gln 171. Notably, Phe 99 (Phe 113 in avian FPPS) has been shown to control product chain length.[13]

The higher potency and superior ligand efficiency (binding energy per ligand atom) of zoledronate[9] can probably be ascribed to the bifurcated H-bonding interaction described above and to the increased rigidity (lower entropic penalty) and bulkiness (additional van der Waals contacts) of the imidazole ring, in comparison with the flexible alkyl chains of other N-BPs. Furthermore, it has been proposed that N-BPs act as transition-state analogues, which mimic the putative carbocation intermediate formed during catalysis.[21] Structural overlays with the avian and *E. coli* FFPS complexes demonstrate that the substituted imidazole nitrogen atom of zoledronate indeed binds in the same region as the putative sp^2-hybridized carbocation. Hence, the increased potency of zoledronate may also derive, in part, from the fact that its imidazole ring is a better transition-state mimetic than the primary or tertiary amino groups of alendronate, pamidronate, and ibandronate.[21]

The 1-OH group of N-BPs, together with the two phosphonate moieties, is responsible for the high affinity of these compounds to bone mineral,[22] thereby targeting these drugs to bone and increasing their efficacy for treating bone diseases. The X-ray crystal structures of the FPPS complexes presented herein suggest that the 1-OH group also contributes to FPPS recognition and binding through a water-mediated hydrogen bond to Gln 240 $O^{\varepsilon}1$ and a direct polar contact with Asp 243 $O^{\delta}2$.

Ternary complex with zoledronate and IPP

The structure of the ternary complex with zoledronate and IPP locates the IPP binding site to a basic region adjacent to the allylic substrate site. IPP binding does not involve any of the DDXXD motifs and is therefore not metal dependent. Three conserved basic residues, Lys 57, Arg 60, and Arg 113, interact directly with the pyrophosphate group of IPP, and three others, Arg 112, Lys 257, and Arg 351, have their positively charged group within 5.0 Å of the pyrophosphate moiety. The hydrocarbon chain of IPP binds between the conserved Phe 239 and the imidazole ring of zoledronate (Figure 4). Several of these residues—Phe 239, Gln 240, Lys 257, and Arg 351—are part of the secondary structural elements that are affected by the conformational switch of FPPS. Hence, the IPP binding site is fully formed only after FPPS is triggered into the partially closed conformation by binding of allylic substrate or N-BP.

Calorimetric data for FPPS–N-BP complexes

Differential scanning calorimetry (DSC) was used to measure the thermal stability of FPPS–N-BP complexes. Parameters such as the melting temperature (T_m) of protein–ligand complexes can be used to compare the binding affinities of different ligands.[23] In our study, zoledronate (T_m 80.6 °C, ΔT_m +25.2 °C)

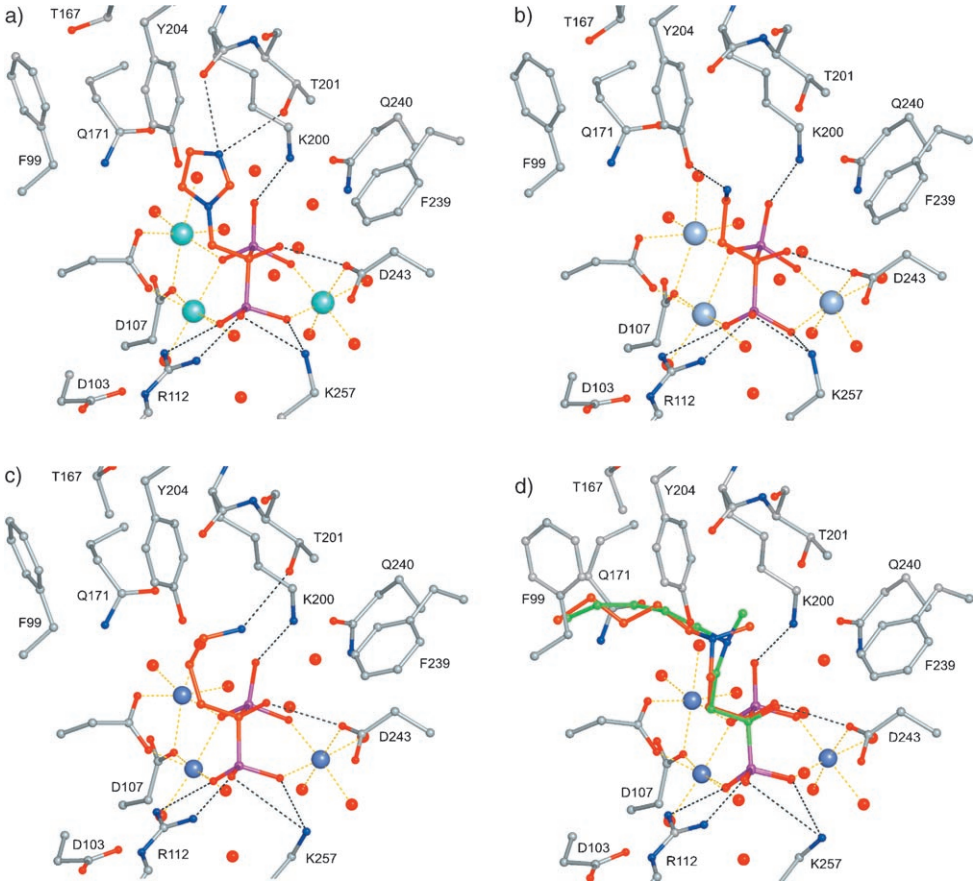

Figure 3. FPPS complexes with a) zoledronate/Mg^{2+}, b) pamidronate/Mn^{2+}, c) alendronate/Zn^{2+}, and d) ibandronate/Zn^{2+}. The metal ions are shown as large spheres. For ease of comparison, all complexes are shown in the same orientation. Black dashed lines show selected hydrogen bonds/electrostatic interactions. Yellow dashed lines show the coordination spheres of the metal ions. The position of the primary amino group of pamidronate was ill-defined in the electron density maps; in this case, one possible orientation is shown which would allow an H-bonding interaction with Tyr 204. For ibandronate, the X-ray crystallographic data indicate that two alternative conformations related by nitrogen inversion are present in the bound state; both conformations are shown. Binding of the ibandronate side chain induces a conformational change of Phe 99, Thr 167, and Gln 171.

was found to induce the largest increase in T_m, followed by risedronate (T_m 76.1 °C, ΔT_m +20.7 °C), ibandronate (T_m 72.6 °C, ΔT_m +17.2 °C), alendronate (T_m 68.9 °C, ΔT_m +13.5 °C), and pamidronate (T_m 64.5 °C, ΔT_m +9.1 °C) as shown in Figure 5a. The ranking of N-BPs by these calorimetric data is in full agreement with enzyme inhibition data using recombinant human FPPS.[9]

The addition of IPP leads to significant further stabilization of FPPS–N-BP complexes (Figure 5b). The T_m value of the FPPS–zoledronate complex increased by 5.0 °C (T_m 85.6 °C) upon addition of IPP. The same phenomenon was observed with other N-BPs. Interestingly, stabilization of the complex upon binding of IPP is more pronounced for weaker N-BPs such as pamidronate (T_m 78.8 °C, ΔT_m +14.3 °C), alendronate (T_m 83.2 °C, ΔT_m +14.3 °C), and ibandronate (T_m 82.9 °C, ΔT_m +10.3 °C) in comparison with stronger binders such as risedronate (T_m 84.4 °C, ΔT_m +8.3 °C) and zoledronate (T_m 85.6 °C, ΔT_m +5.0 °C). As a consequence, differences among the various N-BPs become relatively small in the presence of IPP. Among all the N-BPs studied, zoledronate had the largest stabilizing effect on FPPS in presence or absence of IPP.

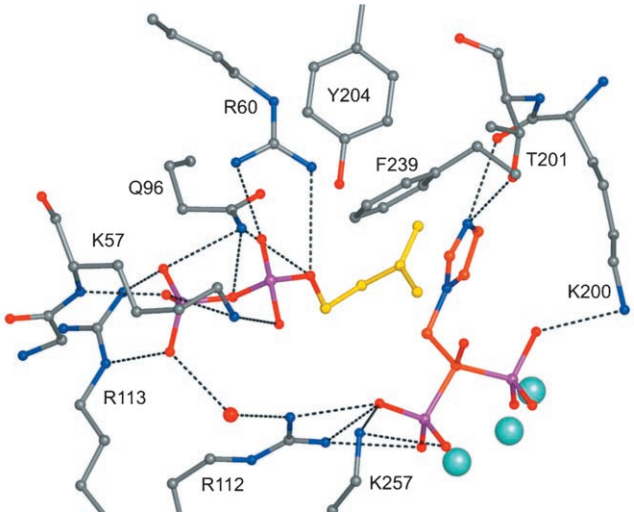

Figure 4. Close-up view of the IPP binding interactions: structure of the ternary complex of human FPPS with IPP (yellow carbon atoms) and zoledronate (orange carbon atoms).

Structural basis for the high in vivo efficacy of N-BPs

Blockade of the FPPS enzymatic activity by zoledronate or other N-BP drugs leads to the intracellular accumulation of the IPP substrate.[8] Therefore, the ternary complex of human FPPS with zoledronate and IPP most likely represents the inhibited form of human FPPS in vivo. As shown above, IPP binds to and further stabilizes the inhibited ternary complex in the fully closed conformation, rather than competing with inhibitor, as in the simple and most frequently observed case of competitive inhibition with single-substrate enzymes (Figure 6). In the fully closed conformation, competition of the N-BP inhibitor by DMAPP/GPP is inefficient, as the N-BP is trapped inside the enzyme, and the allylic substrate binding site is inaccessible (Figure 7 and cover picture). Hence, in addition to other factors such as efficient bone targeting, the high in vivo efficacy and prolonged duration of action of some N-BPs results from the

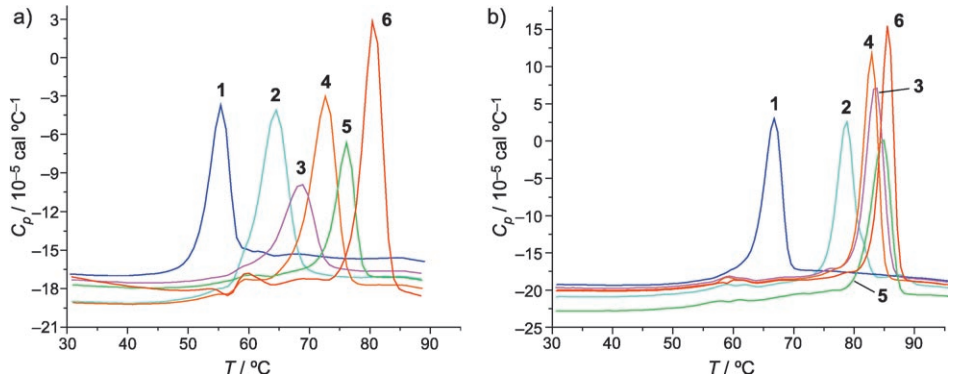

Figure 5. DSC profiles of FPPS–N-BP complexes in the a) absence and b) presence of IPP. The N-BP coding is as follows: 1, FPPS (apo); 2, FPPS–pamidronate; 3, FPPS–alendronate; 4, FPPS–ibandronate; 5, FPPS–risedronate; and 6, FPPS–zoledronate. The concentration of FPPS was 30 μM, of N-BPs 300 μM, and of IPP (for part b only) 300 μM.

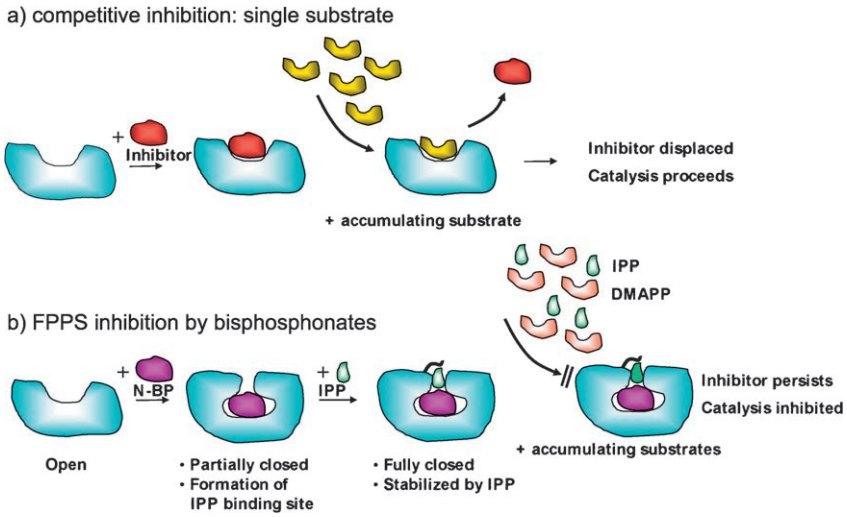

Figure 6. Illustration for the high in vivo efficacy of FPPS inhibition by N-BPs. a) In a competitive inhibition mechanism as with most enzymes, the accumulation of substrate eventually displaces inhibitor, leading to resumption of catalytic activity. b) With FPPS, one of the accumulating substrates (IPP) binds to and further stabilizes the FPPS–N-BP complex, thereby blocking the other substrate (DMAPP) from accessing and displacing the N-BP inhibitor. Suppression of catalysis is thus efficient and sustainable.

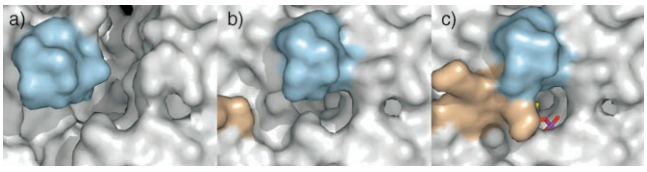

Figure 7. Surface representations of three structural snapshots from the FPPS catalytic cycle: a) open conformation (apo); b) partially closed conformation (zoledronate/Mg^{2+} complex); c) fully closed conformation (zoledronate/Mg^{2+}/IPP complex). Note that in the fully closed conformation, zoledronate is completely shielded from attack by allylic substrate; parts of IPP are visible in panel c).

compulsory-order ternary-complex mechanism of FPPS and the noncompetitive mode of inhibition of N-BPs with respect to the second substrate.

Conclusions

Herein, we describe the first experimental structures of human FPPS.[24] Whereas structures of avian and *S. aureus* FPPS are available only in the open conformation, and of *E. coli* FPPS only in the fully closed conformation, our structures show human FPPS in an open, partially closed, and fully closed conformation and thus provide three snapshots of the enzyme catalytic cycle. One of our major findings is that the stabilization of the inhibitor complex through accumulation of substrate contributes to the high in vivo efficacy of the N-BP drugs.

N-BPs are highly charged hydrophilic compounds. Their pharmacokinetic profile is characterized by high affinity for mineralized bone and prolonged skeletal retention, low exposure in soft tissue, and low permeability across the cell membrane.[6,10] Although FPPS is present in all mammalian cells, the cells primarily targeted by N-BPs in vivo are endocytic or phagocytic cells in bone such as osteoclasts and macrophages, and to a lesser extent renal tubule epithelial cells, as bisphosphonates are excreted exclusively through the kidney. Overall, N-BPs have proven to be well-tolerated, highly efficacious drugs for the treatment of a variety of benign and malignant bone diseases characterized by elevated osteoclastic bone resorption.[1–4,10,25,26]

Although preclinical experiments have convincingly demonstrated antitumour properties of bisphosphonates (reviewed in reference [27]), the results of clinical studies reported to date have been inconsistent and controversial.[28] Likewise, alternative attempts to target the mevalonate pathway and disrupt protein prenylation with inhibitors of farnesyl transferase and geranylgeranyl transferase have also yielded disappointing results in clinical trials.[29] Therefore, it would be of great therapeutic interest to explore the antitumour potential of novel FPPS inhibitors. The currently available N-BPs are not optimal for this purpose for three reasons: first, they have low oral bioavailability (typically ≈1%); second, their pharmacokinetic properties do not permit efficacious drug concentrations to be reached in plasma and soft tissue; and third, these drugs do

not readily enter the cytosol of non-endocytic cells. Our new structural data for human FPPS could facilitate the design of novel inhibitors to overcome these shortcomings; they suggest new avenues toward the discovery of novel FPPS inhibitors such as bisubstrate analogues (such as N-BPs that extend into the IPP site) or allosteric inhibitors (such as compounds that block FPPS in the open state).

The potential therapeutic applications of such novel FPPS inhibitors could extend beyond the treatment of metastatic bone disease to encompass soft-tissue tumours and other diseases such as hypercholesteremia, in which targeting the mevalonate pathway has been shown to be effective. As FPPS is also an essential enzyme in protozoa, bisphosphonates have been proposed as chemotherapeutic agents for the treatment of trypanosomatid and apicomplexan protozoal infections such as Chagas' disease and leishmaniasis.[30,31] The structural data on bisphosphonate binding to trypanosomal FPPS[32] combined with our new data on human FPPS could now facilitate the design of more potent and specific anti-protozoal drugs.

In conclusion, our work opens the possibility for structure-based design of novel FPPS inhibitors that may become a new class of therapeutics directed against a clinically validated target for the treatment of a wide range of diseases.

Experimental Section

Cloning, expression, and purification: Human FPPS (residues 6–353 with an N-terminal His_6 tag followed by a PreScission protease cleavage site) was overexpressed in *E. coli* BL21 (DE3) Tuner cells (Novagen). The soluble fraction of His-tagged FPPS was purified from the cell lysate by anion-exchange (Q-Sepharose HP), hydrophobic (Phenyl Sepharose HP), and metal-chelation (HiTrap) chromatography. The N-terminal His tag was then removed with the PreScission protease, and the reaction products were separated by metal chelation chromatography (HiTrap). His-tag-free FPPS was further purified by size-exclusion chromatography (Superdex-200), concentrated by ultrafiltration to 16 mg mL^{-1}, and stored at −80 °C.

Crystallization and structure solution: All crystals were grown by the vapor-diffusion method at 19 °C from either A) 1.2 M Na/K phosphate (pH 4.7–5.3) with 25% (*v/v*) glycerol or B) 0.1 M zinc acetate, 0.1 M Na acetate, 12% PEG 4000 (pH 4.4). Apo crystals were prepared by mixing equal volumes of crystallization solution A and of a protein stock solution consisting of human FPPS (6-353, 16 mg mL^{-1}) in 25 mM Tris-HCl (pH 8.0), 25 mM NaCl, and 2 mM DTT. The complexes with pamidronate, zoledronate, and IPP were prepared by co-crystallization at a decreased protein concentration (4.2 mg mL^{-1}) in the presence of 5 mM $MgCl_2$ or $MnCl_2$. Stock solutions of pamidronate (50 mM) and zoledronate (10 mM) were prepared in distilled water and added to the enzyme to a final concentration of 2.5 mM and 0.5 mM, respectively. A threefold molar excess of IPP (Sigma) was used. The zinc complexes with zoledronate, alendronate, and ibandronate were prepared by mixing equal volumes of crystallization solution B and a protein stock solu-

Table 1. X-ray data collection and refinement statistics.

Data Set	Free FPPS Open Form	Pamidronate/ Mn^{2+}	Zoledronate/ Mg^{2+}	Zoledronate/ Zn^{2+}	Zoledronate/ IPP/Mg^{2+}	Alendronate/ Zn^{2+}	Ibandronate/ Zn^{2+}
				Data Collection			
Wavelength [Å]	0.97933	1.00003	1.00003	1.00003	1.00033	1.00003	1.00003
Space Group	$P4_12_12$	$P4_12_12$	$P4_12_12$	$P4_12_12$	$P4_12_12$	$P4_12_12$	$P4_12_12$
Unit Cell	$a=b=110.89$	$a=b=111.57$	$a=b=111.84$	$a=b=111.27$	$a=b=112.16$	$a=b=111.50$	$a=b=111.35$
Dimensions [Å]	$c=77.00$	$c=66.48$	$c=66.04$	$c=69.03$	$c=65.72$	$c=70.22$	$c=68.89$
No. Subunits/a.u.	1	1	1	1	1	1	1
Resolution Range	100.0–2.30	100.0–2.60	100.0–2.20	100.0–2.06	100.0–2.60	100.0–2.15	50.0–1.94
(Highest Shell) [Å]	(2.37–2.30)	(2.69–2.60)	(2.28–2.20)	(2.13–2.06)	(2.69–2.60)	(2.21–2.15)	(2.00–1.94)
Redundancy	14.3	13.4	14.3	14.2	7.7	7.1	13.4
Completeness [%]	99.5 (99.9)	99.9 (99.8)	99.8 (100)	99.7 (99.8)	99.9 (100)	99.5 (99.7)	99.2 (96.3)
I/σ (I)	23.3	8.0	10.8	21.2	8.8	15.8	24.3
R_{merge}	0.072 (0.325)	0.070 (0.434)	0.055 (0.423)	0.079 (0.382)	0.072 (0.481)	0.068 (0.466)	0.066 (0.422)
				Refinement			
Resolution Å	41.7–2.30	57.1–2.60	56.9–2.20	49.8–2.06	56.7–2.61	40.7–2.15	40.4–1.94
No. Reflections	21795	13389	21775	27286	13212	24529	32351
R_{work}/R_{free}	0.225/0.257	0.199/0.267	0.217/0.268	0.209/0.259	0.220/0.280	0.247/0.289	0.205/0.241
				No. Atoms			
Protein	2758	2806	2775	2775	2806	2775	2766
Ligand	–	13	16	16	30	14	2×19
Water	54	54	135	164	61	100	207
$Mn^{2+}/Mg^{2+}/Zn^{2+}$	–	3	3	3	3	3	3
Mean B Factor [Å^2]	64.0	69.9	55.1	42.7	59.9	45.4	39.2
				rms Deviations			
Bond Length [Å]	0.007	0.007	0.007	0.006	0.007	0.007	0.007
Bond Angle [°]	1.0	1.1	1.1	0.9	1.2	1.0	1.0

tion consisting of human FPPS (6-353, 14 mg mL^{-1}) in 10 mM Tris (pH 7.4), 25 mM NaCl, 5 mM $MgCl_2$, and 1.0 mM bisphosphonate.

X-ray crystallographic data collection and structure determination: Crystallographic data were collected at 95 K with a MARCCD detector and synchrotron radiation (Swiss Light Source, beam line XS06A). The crystals were mounted in cryoloops and flash-frozen. For the zoledronate, alendronate, and ibandronate complexes with Zn^{2+}, a cryoprotectant made of 20% glycerol and 80% well solution was used. Diffraction data were recorded as 1.0° oscillation images and processed with HKL[33] or XDS.[34] All crystals were in space group $P4_12_12$ with one FPPS monomer per asymmetric unit. The structure of human FPPS (open form) was initially determined by molecular replacement with the program AMoRe[35] with avian FPPS (PDB code: 1FPS) as a search model. The structure was then refined with CNX[36] and O.[37] The structures of the FPPS complexes were determined by using an initial rigid-body refinement of the apo structure followed by full refinement with CNX and O. Data collection and refinement statistics are summarized in Table 1. All refined structures have been deposited into the Protein Data Bank, with entry codes 2F7M (unliganded FPPS), 2F89 (pamidronate/Mn^{2+} complex), 2F8C (zoledronate/Mg^{2+} complex), 2F9K (zoledronate/Zn^{2+} complex), 2F8Z (zoledronate/IPP/Mg^{2+} complex), 2F92 (alendronate/Zn^{2+} complex), and 2F94 (ibandronate/Zn^{2+} complex).

Differential scanning calorimetry (DSC): DSC scans were obtained with a MicroCal VP-capDSC system (MicroCal LLC, Northampton, MA, USA) operated at a scan rate of 200 °C h^{-1}. The final FPPS concentration was typically 30 μM in 25 mM Tris (pH 7.5), 25 mM NaCl and 5 mM $MgCl_2$. N-BPs and IPP (Echelon Inc., Salt Lake City, UT, USA) were added to the protein solution at a final concentration of 300 μM.

Note added in proof: After this manuscript was submitted, structural data for FPPS from *T. cruzi* were published (S. B. Gabelli, J. S. McLellan, A. Montalvetti, E. Oldfield, R. Docampo, L. M. Amzel, *Proteins: Struct. Funct. Bioinf.* **2006**, *62*, 80) which fully corroborate the findings presented herein.

Acknowledgement

We thank Drs. René Amstutz and Hans Widmer for their continued support, Armin Widmer for computational support, Damien Begue for technical support, and Dr. Ulf Neumann for helpful discussions. X-ray crystallographic data collection was performed at the Swiss Light Source, Paul Scherrer Institut, Villigen, Switzerland. We are grateful to the machine and beamline groups whose outstanding efforts have made these experiments possible.

Keywords: bone metastasis · drug design · farnesyl pyrophosphate synthase · inhibitors · osteoporosis

[1] P. D. Delmas, *Lancet* **2002**, *359*, 2018.
[2] A. L. Langston, S. H. Ralston, *Rheumatology* **2004**, *43*, 955.
[3] J. R. Berenson, *Semin. Oncol.* **2002**, *29*, 12.
[4] R. E. Coleman, *Oncologist* **2004**, *9, Suppl 4*, 14.
[5] J. E. Fisher, G. A. Rodan, A. A. Reszka, *Endocrinology* **2000**, *141*, 4793.
[6] M. J. Rogers, S. Gordon, H. L. Benford, F. P. Coxon, S. P. Luckman, J. Monkkonen, J. C. Frith, *Cancer* **2000**, *88*, 2961.
[7] E. van Beek, E. Pieterman, L. Cohen, C. Lowik, S. Papapoulos, *Biochem. Biophys. Res. Commun.* **1999**, *264*, 108.
[8] J. D. Bergstrom, R. G. Bostedor, P. J. Masarachia, A. A. Reszka, G. Rodan, *Arch. Biochem. Biophys.* **2000**, *373*, 231.
[9] J. E. Dunford, K. Thompson, F. P. Coxon, S. P. Luckman, F. M. Hahn, C. D. Poulter, F. H. Ebetino, M. J. Rogers, *J. Pharmacol. Exp. Ther.* **2001**, *296*, 235.
[10] A. A. Reszka, G. A. Rodan, *Mini-Rev. Med. Chem.* **2004**, *4*, 711.
[11] C. D. Poulter, H. C. Rilling, *Acc. Chem. Res.* **1978**, *11*, 307.
[12] L. C. Tarshis, M. Yan, C. D. Poulter, J. C. Sacchettini, *Biochemistry* **1994**, *33*, 10871.
[13] L. C. Tarshis, P. J. Proteau, B. A. Kellogg, J. C. Sacchettini, C. D. Poulter, *Proc. Natl. Acad. Sci. USA* **1996**, *93*, 15018.
[14] D. J. Hosfield, Y. Zhang, D. R. Dougan, A. Broun, L. W. Tari, R. V. Swanson, J. Finn, *J. Biol. Chem.* **2004**, *279*, 8526.
[15] F. H. Ebetino, C. N. Roze, C. E. McKenna, B. L. Barnett, J. E. Dunford, R. G. G. Russell, G. E. Mieling, M. J. Rogers, *J. Organomet. Chem.* **2005**, *690*, 2679.
[16] L. Song, C. D. Poulter, *Proc. Natl. Acad. Sci. USA* **1994**, *91*, 3044.
[17] J. E. Coleman, *Annu. Rev. Biophys. Biomol. Struct.* **1992**, *21*, 441.
[18] A. Volbeda, A. Lahm, F. Sakiyama, D. Suck, *EMBO J.* **1991**, *10*, 1607.
[19] D. J. Hosfield, Y. Guan, B. J. Haas, R. P. Cunningham, J. A. Tainer, *Cell* **1999**, *98*, 397.
[20] E. Hough, L. K. Hansen, B. Birknes, K. Jynge, S. Hansen, A. Hordvik, C. Little, E. Dodson, Z. Derewenda, *Nature* **1989**, *338*, 357.
[21] M. B. Martin, W. Arnold, H. T. Heath, 3rd, J. A. Urbina, E. Oldfield, *Biochem. Biophys. Res. Commun.* **1999**, *263*, 754.
[22] E. R. van Beek, C. W. Lowik, F. H. Ebetino, S. E. Papapoulos, *Bone* **1998**, *23*, 437.
[23] T. T. Waldron, K. P. Murphy, *Biochemistry* **2003**, *42*, 5058.
[24] The structural coordinates of human FPPS complexes were recently deposited into the PDB by Kavanagh et al. Although no published manuscript is available, these structures are in agreement with the more comprehensive findings and conclusions described herein.
[25] a) E. Kotsikorou, E. Oldfield, *J. Med. Chem.* **2003**, *46*, 2932; b) L. Widler, K. A. Jaeggi, M. Glatt, K. Muller, R. Bachmann, M. Bisping, A. R. Born, R. Cortesi, G. Guiglia, H. Jeker, R. Klein, U. Ramseier, J. Schmid, G. Schreiber, Y. Seltenmeyer, J. R. Green, *J. Med. Chem.* **2002**, *45*, 3721.
[26] M. J. Rogers, *Curr. Pharm. Des.* **2003**, *9*, 2643.
[27] P. Clezardin, P. Fournier, S. Boissier, O. Peyruchaud, *Curr. Med. Chem.* **2003**, *10*, 173.
[28] H. L. Neville-Webbe, I. Holen, R. E. Coleman, *Cancer Treat. Rev.* **2002**, *28*, 305.
[29] F. Caponigro, M. Casale, J. Bryce, *Expert Opin. Invest. Drugs* **2003**, *12*, 943.
[30] R. Docampo, S. N. Moreno, *Curr. Drug Targets Infect. Disord.* **2001**, *1*, 51.
[31] L. R. Garzoni, M. C. Waghabi, M. M. Baptista, S. L. de Castro, N. Meirelles Mde, C. C. Britto, R. Docampo, E. Oldfield, J. A. Urbina, *Int. J. Antimicrob. Agents* **2004**, *23*, 286.
[32] J. Mao, Y. G. Gao, S. Odeh, H. Robinson, A. Montalvetti, R. Docampo, E. Oldfield, *Acta Crystallogr. Sect. D* **2004**, *60*, 1863.
[33] Z. Otwinowski, W. Minor, *Methods Enzymol.* **1997**, *276*, 307.
[34] W. Kabsch, *J. Appl. Crystallogr.* **1993**, *26*, 795.
[35] J. Navaza, *Acta Crystallogr. Sect. A* **1994**, *50*, 157.
[36] A. T. Brunger, P. D. Adams, G. M. Clore, W. L. DeLano, P. Gros, R. W. Grosse-Kunstleve, J.-S. Jiang, J. Kuszewski, M. Nilges, N. S. Pannu, R. J. Read, L. M. Rice, T. Simonson, G. L. Warren, *Acta Crystallogr. Sect. D* **1998**, *54*, 905.
[37] T. A. Jones, J. Y. Zou, S. W. Cowan, M. Kjeldgaard, *Acta Crystallogr. Sect. A* **1991**, *47*, 110.

Received: October 7, 2005

